ChemistrySelect

Full Papers
doi.org/10.1002/slct.202000432

Chemistry
Europe
European Chemical
Societies Publishing

▐ **Materials Science inc. Nanomaterials & Polymers**

Preparation of Amine- and Disulfide-Containing PAMAM-Based Dendrons for the Functionalization of Hydroxylated Surfaces: XPS as Structural Sensor

Herlys Viltres,[a] Oscar F. Odio,*[b] Mark. C. Biesinger,[c] Gala Montiel,[d] Raúl Borja,[e] and Edilso Reguera*[a]

Herein, we report the synthesis of novel poly(amido amine) [PAMAM]-based dendrons with external amine and disulfide functional groups and an alkoxysilane moiety as the focal point. Four generations (**G1-G4**) of dendrons were obtained by combining Michael addition and amidation reactions using (3-aminopropyl) trimethoxysilane as the starting core; disulfide bridges and amine groups were introduced in the last step by ester amidation with cystamine and ethylendiamine. The resulting dendrons were characterized by Thermogravimetric Analysis (TGA), Fourier Transform Infrared (FTIR), Raman, Atomic Force Microscopy (AFM), Dynamic Light Scattering (DLS) and Z-potential techniques. The growth of the dendrons was monitored by analysing the X-ray Photoelectron Spectroscopy (XPS) high resolution spectra of the Si 2p, N 1s, C 1s, O 1s and S 2p signals for each dendron generation. The results evidence that it is possible to record, with good confidence, the compositional and structural changes that occur during the preparative route by means of XPS technique.

1. Introduction

Polymer surface analysis is relevant in many scientific fields since its composition and structure influence key properties like wettability,[1] adhesion,[2] biological activity[3] and photoluminescence.[4] Moreover, recent research efforts have been focused on the design of advanced polymeric materials with specific surface functionalities that could be used in several applications like environmental remediation,[5] biomedicine[6] and catalysis.[7] In order to get insights about the surface properties of polymeric and polymer-containing hybrid materials, surface characterization techniques are required. Among them, X-ray photoelectron spectroscopy (XPS) has become crucial for polymer surface analysis since it provides useful chemical information, including the presence of functional groups and interfacial interactions.[8]

Dendrimers are novel, nanostructured synthetic polymers that possess a highly branched structure with a unique three-dimensional molecular configuration and a large number of chemical functionalities,[3b,9] which are able to react with other species at the nanoscale. Between the branches of dendrimers, also called dendrons, there are a large number of empty cavities which can trap or encapsulate different compounds like drugs and pollutants.[5d,10] An individual dendron usually contains a single chemically addressable group called the focal point or core. Either dendrimers or individual dendrons can be synthetically grown from a small molecule that is subjected to iterative reaction sequences resulting in new molecular generations with increasing diameter, molecular weight and number of functional end groups.[5d]

Poly(amidoamine) [PAMAM] is one of the most extensively studied dendrimer with diverse applications and current research interest in supramolecular chemistry.[11] The main features of PAMAM and its derivatives include: (1) interior amine and amide groups that can interact with ionic metal precursors through coordination chemistry or ligand-exchange reactions; (2) interior void space and structural flexibility that can accommodate supramolecular guest species; and (3) exterior chemical groups (amine, hydroxyl, carboxyl, etc.) that permit further functionalization, tethering to surfaces and assembly into higher-order structures.[5d] Also, it was evidenced in diverse studies the great potential to be used in several applications[12] like drug delivery,[13] tissue engineering,[6a,14] bio-imaging,[15] catalysis,[16] cancer therapy,[17] imaging agents,[18] and water remediation.[5d,19]

This work describes the preparation and structural characterization of novel and versatile dendrons with (3-aminopropyl)trimethoxysilane (APTMS) as the focal point and disulfide and amine functions as terminal groups. The alkoxysilane core is intended to favor dendron anchorage to materials with hydroxylated surfaces like Al_2O_3, SiO_2, TiO_2 and iron oxide

[a] Dr. H. Viltres, Prof. E. Reguera
Centro de Investigación en Ciencia Aplicada y Tecnología Avanzada-Unidad Legaria, Instituto Politécnico Nacional, Ciudad de México, México
E-mail: edilso.reguera@gmail.com

[b] Dr. O. F. Odio
CONACyT-Instituto Politécnico Nacional, Centro de Investigación en Ciencia Aplicada y Tecnología Avanzada, Unidad Legaria, Ciudad México, México
E-mail: odiochacon@gmail.com

[c] Dr. M. C. Biesinger
Surface Science Western, Western University, Ontario, Canada

[d] G. Montiel
Universidad de la Salle, Ciudad de Mexico, Mexico.

[e] Dr. R. Borja
Centro de Nanociencias y Micro-Nanotecnologías, Instituto Politécnico Nacional, Ciudad de México, Distrito Federal, México.

💻 Supporting information for this article is available on the WWW under https://doi.org/10.1002/slct.202000432

ChemistrySelect

Full Papers
doi.org/10.1002/slct.202000432

Chemistry Europe
European Chemical
Societies Publishing

nanoparticles; at the same time, the —S—S— bridges are a potential source of free —SH moieties, which in conjunction with —NH$_2$ terminal groups could either promote several supramolecular reactions or capture important water pollutants like heavy metal cations and arsenic species. Dendrons were characterized by FTIR, Raman, TGA, AFM and DLS. We devote particular emphasis on XPS since it is employed for monitoring the dendron growth by analysing the evolution of the terminal functions and the surface interactions. As far as we know, this is one of the few reports that make use of the XPS technique for such endeavor.[20]

2. Results and Discussion

2.1 Dendron structural characterization

The synthesis of amine-functionalized dendrons of generation 1–4 has been previously published using 2-(2-Amino-ethoxy)-ethanol as initial core.[21] A similar methodology with some improvements and changes was applied to obtain two fourth-generation dendrons with amine and disulfide moieties at the periphery and silane groups at the focal point (**D-G4** and **D-G4.1**, see Figure 1A). These dendrons were grown by sequential Michael addition of methyl acrylate to primary amines followed by ester amidation with a large excess of ethylendiamine (EDA). We use APTMS as the starting compound (or zero generation), which could allow an efficient dendron anchoring to different hydroxylated surfaces, while amine and thiol terminals bring
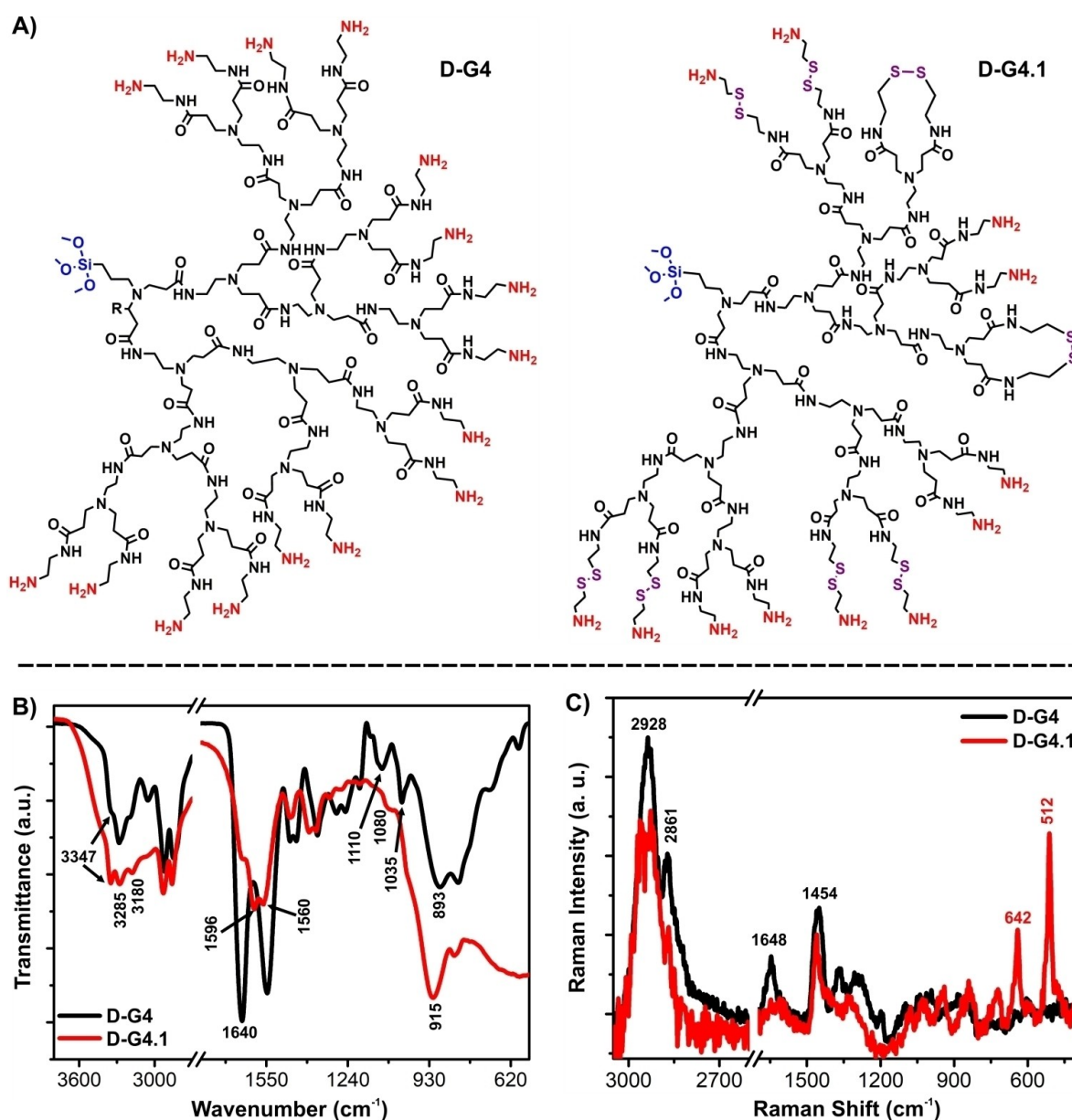

Figure 1. A) Likely structures of compounds **D-G4** and **D-G4.1**. **B)** FT-IR and **C)** Raman spectra of **D-G4** and **D-G4.1** samples.

ChemistrySelect

Full Papers
doi.org/10.1002/slct.202000432

Chemistry Europe
European Chemical
Societies Publishing

versatility to the hybrid material for multiple applications. Instead of the direct incorporation of –SH groups, we prefer to introduce disulfide bridges as thiol protecting groups[22] using cystamine (Cys) in the last amidation step, in order to avoid undesirable secondary reactions of thiols during the dendron synthesis; within this approach, free thiols can be obtained by a facile reduction step just before the desired application.[23] The final yields (around 91%) are higher respect for those proposed in the literature.[21] Details of the synthesis procedures are provided in the Supporting Information.

Figure 1B shows the FT-IR spectra of **D-G4** and **D-G4.1** samples (all spectra can be found in the Supporting Information). Both spectra are dominated by the signals coming from amine and amide functions. Thus, the peaks at 3347 and 3289 cm^{-1} are related to the asymmetric and symmetric stretching vibrations ascribed to -NH$_2$ groups; meanwhile, the signal around 3180 cm^{-1} is attributed to the stretching vibration of N—H from secondary amides in the structure. The peaks at 1640 cm^{-1} correspond to the stretching vibration of C=O group in amide functions, while the peaks at 1596 and 1560 cm^{-1} are ascribed to the bending modes ($\delta^s_{NH_2}$) of amines and amides, respectively. Also, the peaks at 1110 and 1080 cm^{-1} are due to the stretching vibrations of C—N bond, and the wide bands at 893 and 915 cm^{-1} are due to the bending vibration of -NH$_2$ ($\gamma^s_{NH_2}$). Besides, the small peak in **D-G4** around 1035 cm^{-1}, which is seen as a shoulder in **D-G4.1** sample, can be ascribed to the C—O—Si stretching vibrations in the alkoxysilane group acting as dendron core; this signal can be better observed for smaller dendron generations. It is worth to mention the absence in both spectra of the signals corresponding to ester functions, which indicates the quantitative conversion of the intermediate product **D-G3.5**. Indeed, the occurrence of these bands (specially the C=O stretching vibration near 1730 cm^{-1}) senses the extent of the amidation step and dictates the necessity for an extra addition of EDA in order to amidate the remaining ester functions. In the case of the series **D-G2** to **D-G4**, the unreactive ester groups are due to the increasing steric hindrance between the dendron chains that hamper the proper approach of EDA molecules; in the case of the synthesis of **D-G4.1**, this hampering becomes more important due to the larger size of Cys compared with EDA.

Figure 1C presents the Raman spectra of **D-G4** and **D-G4.1** samples. Both are very similar, but the spectrum corresponding to **D-G4.1** exhibits two new sharp peaks at 512 and 642 cm^{-1}, which are assigned to the S—S and C—S stretches, respectively. Therefore, it can be confirmed the incorporation of Cys molecules into the dendron structure. By calculating the free thiol content in the sample through UV-vis spectrophotometry, it was estimated a disulfide concentration of 4.4 mmol per gram of dendron (see Supporting Information). Other important features can be mentioned in the Raman spectra. For instance, the signals at 2928 and 2861 cm^{-1}, as well as the peak at 1454 cm^{-1} account for the stretching and scissoring modes of the –CH$_2$ groups in the dendron skeleton; also, it is possible to identify the band related to amide groups at 1648 cm^{-1}. These results support the presence of amine and disulfide functionalities present in the PAMAM dendrons, including the

retention of the alkoxysilane group as focal point. More insights on dendron composition and functional groups are discussed below.

The dendron growth sequence was studied by the TGA of the complete generations (see in Figure 2A the structures of **D-G1** to **D-G3** compounds). Figure 2B shows the resulting thermogravimetric curves. For all cases, there is a minor weight loss (less than 20%) in the temperature range 100–120 °C due to the evaporation of traces of methanol, physisorbed water or EDA. The major weight loss occurs in the temperature range 200–400 °C, corresponding to the decomposition of the dendron organic skeleton, leaving SiO$_2$ as the expected residue (see Table 1 in the Supporting Information). It is observed that the extent of the organic decomposition increases with the generation number, which indicates the effective dendron growth. Note that the organic decomposition step is more extensive for **D-G2** compared to **D-G1**, which is in agreement with a sudden increase in the organic content relative to the alkoxysilane group; however, as the dendron generation increases, the extent of organic decomposition becomes similar due to the minority content of the alkoxysilane group. This trend is clearly observed from Figure 1C, where the fraction of weight loss due to dendron decomposition (corrected for the minor weight loss) is plotted against the estimated carbon content (in mol basis) for each dendron generation.

Besides, a close inspection of the profiles makes apparent that dendron skeleton begins to decompose at lower temperature as the generation is higher, which is likely related with an increase in the chain flexibility with the molecular size; on the contrary, **D-G4** becomes thermally stiffer when disulfide bridges are introduced in the chains, in agreement with previous reports,[24] suggesting that some Cys molecules are acting as cross-linking agents between branches or dendron molecules (see Figure 1A *right*). In fact, the difference in the thermograms between **D-G4** and **D-G4.1** indicates the successful introduction of disulfide functions.

Figure 3 (*top*) shows the AFM topography images in PeakForce Tapping mode[25] of the samples **D-G2**, **D-G3** and **D-G4** after evaporation of the methanol solutions. **D-G2** micrograph exhibits flattened and irregular dendron aggregates with an average diameter of 36 nm and a height around 1.1 nm; this behavior has been reported before for initial dendrimer generations.[26] The rather open structure of these small dendrons allows for the interpenetration of the branches, which gives rise to individual aggregates with an irregular shape. On the contrary, **D-G3** and **D-G4** samples show a markedly different morphology with a ring-like shape resembling a donut. Interestingly, the average ring thickness are very similar (32 nm for **D-G3** and 36 nm for **D-G4**) to the average aggregate size in **D-G2**; this fact suggests that as the dendron skeleton becomes more compact and stiffer due to the increasing number of branches, the initial aggregates tend to self-organize during solvent evaporation through intermolecular interactions between the external functional groups. It seems that the final ring-like shape results from the complex hydrophilic/hydrophobic balance between dendron-dendron and substrate-dendron interactions.[27] Additional confirmation
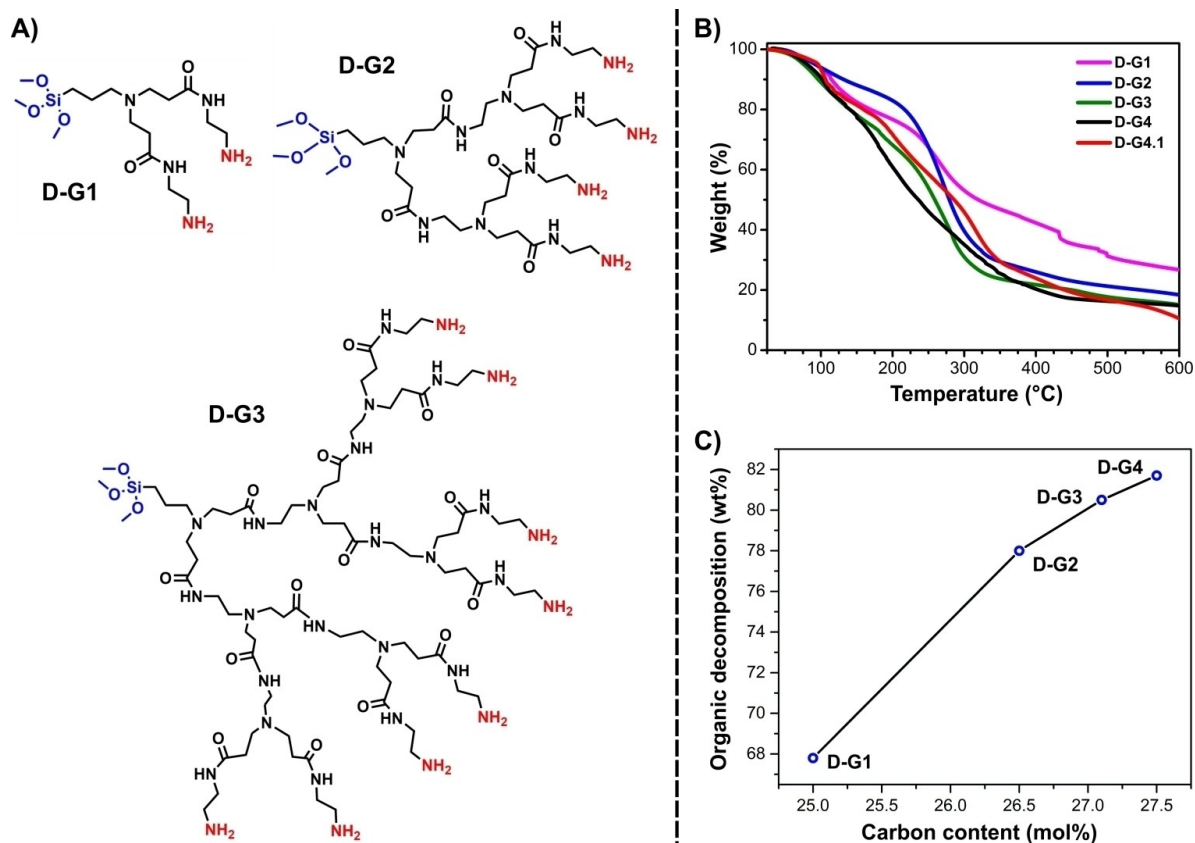
ChemistrySelect

Full Papers
doi.org/10.1002/slct.202000432

**Chemistry
Europe**
European Chemical
Societies Publishing

Figure 2. A) Likely structures of compounds **D-G1** to **D-G3**. **B)** TGA thermograms for complete generations of PAMAM dendrons. **C)** Correlation between the weight loss due to organic decomposition and the carbon content for **D-G1** to **D-G4**.

about these supramolecular interactions can be obtained from the STEM image of **D-G4** sample after methanol evaporation (see the Supporting Information); it shows the presence of near spherical aggregates (average diameter around 32 nm) not randomly distributed, but rather interconnected in a self-organized way. It is important to stress that both AFM and STEM do not necessarily give the same self-organizing pattern, since in each technique the substrate is quite different.

The increasing size of the dendron generations can also be envisaged by determining the average height of the aggregates. As can be seen in Figure 3 (*center*), for the three samples the aggregate height follows a Gaussian distribution; there is an increase in *c.a.* 1 nm from one generation to another with mean heights of 1.1, 2.1 and 3.2 nm for **D-G2**, **D-G3** and **D-G4**, respectively. At the same time, it is observed an increase in the narrowness of the size distribution. It is worth to note that the measured height is likely underestimated, since the interfacial interactions between the dendron external polar groups and the glass substrate promote the spreading out of the macromolecules, especially for low dendron generations.[26,28] This flattening of the samples is substantially attenuated in the STEM image since the dendron solution is cast over a hydrophobic carbon-coated copper grid.

DLS provides information about the hydrodynamic size of the dendritic structures in solution (see Figure 3A) *bottom*.

Diameters range from 1.9 to 4.6 nm, with low polydispersity index (0.22-0.23). From the obtained values it follows that as the molecular size increases, the hydration sphere is more extensive; this is consistent with the increase in the number of polar end groups that favor dendron-water interactions. As can be seen, both AFM and DLS evidence the expected increase in dendron size with the number generation.

Zeta-potential measurements provide further hints about the colloidal stability of the dendrons. From Figure 3B (*bottom*) it follows that at pH 6 the zeta-potential increases monotonically from **D-G1** to **D-G4** (12.3 to 17.4 mV); such trend in the positive values accounts for the increasing number of amine groups that are protonated at pH 6. Since for PAMAM dendrimer the outer primary amine groups ($pK_{HA} = 7-9$) are more basic that the internal tertiary amines ($pK_{HA} = 3-6$),[29] it is expected that at pH 6 the protonated nitrogen atoms mainly come from the exterior groups. Another hint confirming that surface amine protonation is the leading mechanism for colloidal stabilization is given by the fact that for **D-G3.5** sample, which does not present terminal amine groups but ester functions, the zeta-potential drops to near zero (-4.7 mV). The influence of pH in the colloidal stability of **D-G4** sample was also studied. As can be noted in Figure 3C (*bottom*), the zeta-potential decreases smoothly as the pH gets higher in the interval 2–6 and then suffers a sudden decrease at pH 7,
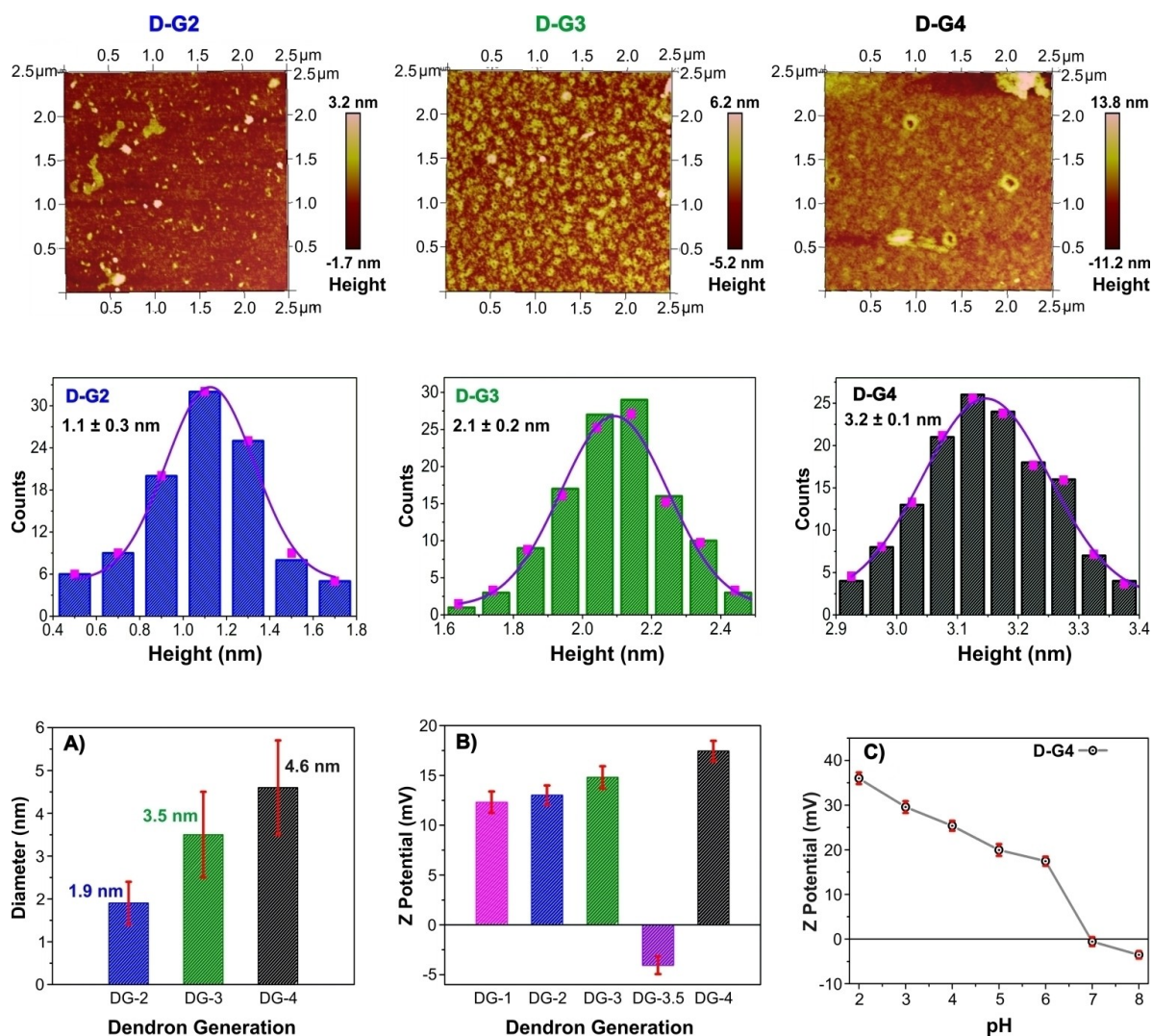
ChemistrySelect

Full Papers
doi.org/10.1002/slct.202000432

Chemistry Europe
European Chemical
Societies Publishing

Figure 3. AFM topography images (*Top*) for several dendrons with the corresponding height distributions (*Center*). *Bottom*: A) Hydrodynamic diameter and at pH 7; B) Z-potential for selected dendrons at pH 6; C) Variation of the Z-potential of **D-G4** dendron as function of pH (vertical bars account for the standard deviation of the data).

suggesting that at this point amine protonation is no longer favored in the acid-base equilibrium, provoking colloidal instability. This behaviour is consistent with the protonation of external amine groups as the source for surface positive charges that impart colloidal stability to the dendrons.

2.2. Dendron surface characterization by XPS

XPS analysis was carried out aiming to study the composition of different dendron generations. Although we are aware that other techniques are customarily used for dendron characterization, we focus on XPS since the dendrons we are dealing with are devoted to potential applications where the molecules are grown at the surface of functional materials; hence, in these cases surface-sensitive techniques are the best option to study the structure and composition of organic coating layers. Moreover, XPS can provide information related with interac-

tions that lead to important interfacial phenomena like adsorption or binding processes. The XPS survey scans for the samples under study clearly display the C 1s, O 1s, N 1s and Si 2p signals, as well as the presence of a new peak at 163 eV for S 2p in **D-G4.1** sample (see Table 2 in the Supporting Information), which corroborates the incorporation of Cys molecules into the dendron structure. Also, element quantification gives similar results to those calculated from the theoretical estimation of the dendron composition, which confirms the good agreement between the proposed molecular composition and the final products obtained. In order to gather deeper information about dendron composition and structure, we collected and analysed high-resolution XPS spectra. All spectral fitting parameters are summarized in Tables 3–7 of Supporting Information. For the discussion herein, we selected the samples **D-G1**, **D-G2**, **D-G4** and **D-G4.1**.

ChemistrySelect

Full Papers
doi.org/10.1002/slct.202000432

Chemistry
Europe
European Chemical
Societies Publishing

Figure 4A shows the Si 2p curve fitting for the first obtained dendrons (**D-G0.5** and **D-G1**). Both spectra are fitted with one contribution consisting in a doublet separated by 0.6 eV due to the spin-orbit coupling. For **D-G0.5**, the Si 2p3/2 signal is centred at 102.0 eV, while for **D-G1** the same signal is slightly shifted to 102.4 eV; both binding energy values can be assigned to an $Si(-O)_3$ environment that matches with the APTMS initial core.[8c,30] However, it is worth to note that the small increase in the binding energy is maintained for higher dendron generations, for which a small increase in the signal width is also recorded (see Table 3 in the Supporting Information). Such facts might suggest that there occur subtle changes in the Si environment after the second reaction step. A likely process that is typical for alkoxysilanes is alcohol condensation to give siloxanes ($-Si-O-Si-)_n$; in fact, the substitution of an alkyl carbon by a Si atom is consistent with a small increase in the Si 2p binding energy, since the new Si–O–Si bonds present a less covalent character than the initial Si–O–C bonds. Therefore, it could be plausible to state that during the amidation of **D-G0.5** dendrons, a fraction of the APTMS cores is forming a siloxane network due to the condensation of adjacent focal points (see Figure 4B).[30b,31] It is known that the hydrolysis of methoxyl groups from APTMS into hydroxy groups occurs in the presence of water even in trace quantities; then, the hydrolyzed APTMS can condense with neighbor silanol groups forming either a monolayer or a less probable highly branched polycondensed structure. This result allows proposing that two or more dendrons could be linked togetherfrom their focal points, due to the appearance of the polysiloxane contribution in the XPS fits. Such phenom-

enon could be important since for many applications the amount of dendron anchored to the surface is a critical variable, which in turn depends on the amount of hydrolizable free alkoxy groups.

The N 1s core-level spectra of selected dendrons are shown in Figure 5 (*left*). The profiles are fitted with three component peaks centered at 399.3–399.5 eV, 399.7–399.9 eV and 401.3–401.8 eV. The first major contribution can be attributed to primary and tertiary amine (R–C-N) groups, while the second major contribution corresponds to the amide (N-C=O) groups belonging to the dendron structure.[8c,32] The minoritory contribution at higher binding energy can be related with amine nitrogen atoms bearing a partial or net positive charge, arising either due to the occurrence of inter and intra-molecular hydrogen bonds or the protonation of amines by water traces.[33] Amine participation in this contribution is supported by the fact that the signal area increases as the dendron generation is higher. Also, since the signal area is depleted for intermediate generations (see Table 4 in the Supporting Information), it is likely that the contribution mainly entails the external primary amines, which is consistent with a higher amine basicity respect to the internal tertiary amines. A schematic representation of the possible interactions of amine terminals that contribute to this third contribution is presented in Figure 6A.

Figure 6B (circles) shows the experimental variation of the area ratio between amine and amide signals compared with the theoretical values based on the proposed structures. As it is apparent, there is a close agreement between both data sets, indicating that XPS analysis provides confident results about
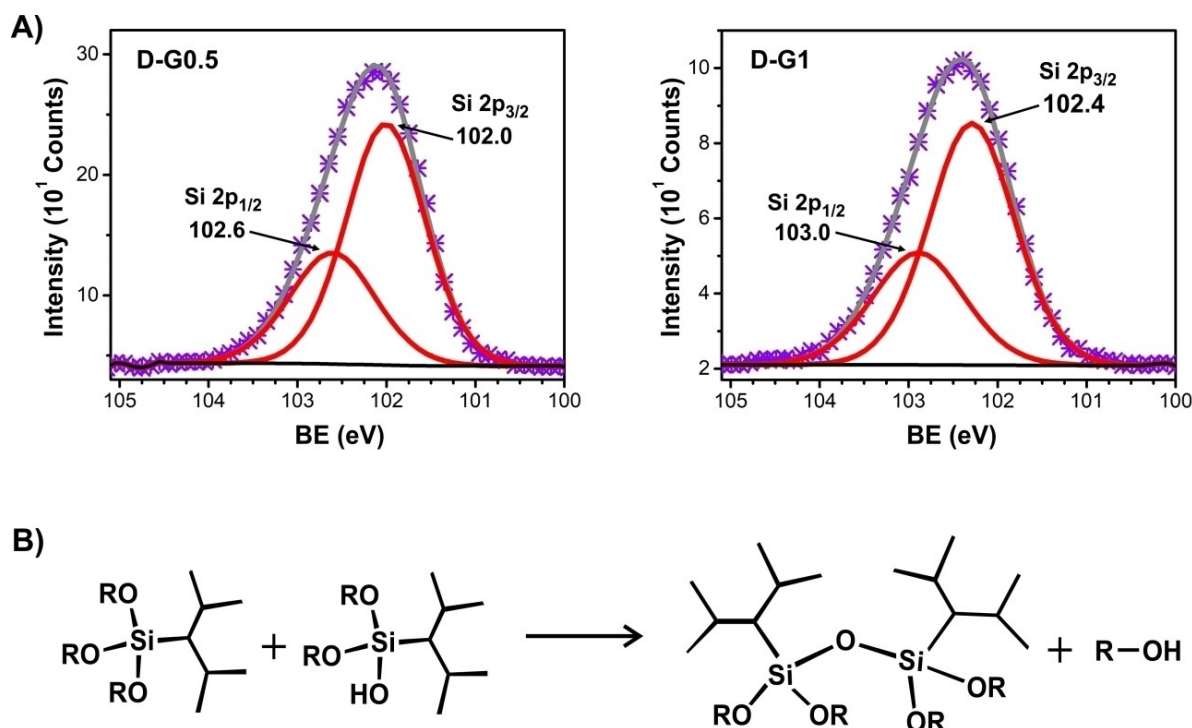

Figure 4. A) XPS high-resolution spectra of Si 2p for **D-G0.5** and **D-G1** dendrons. **B)** Schematic representation of the condensation of alkoxysilanes.
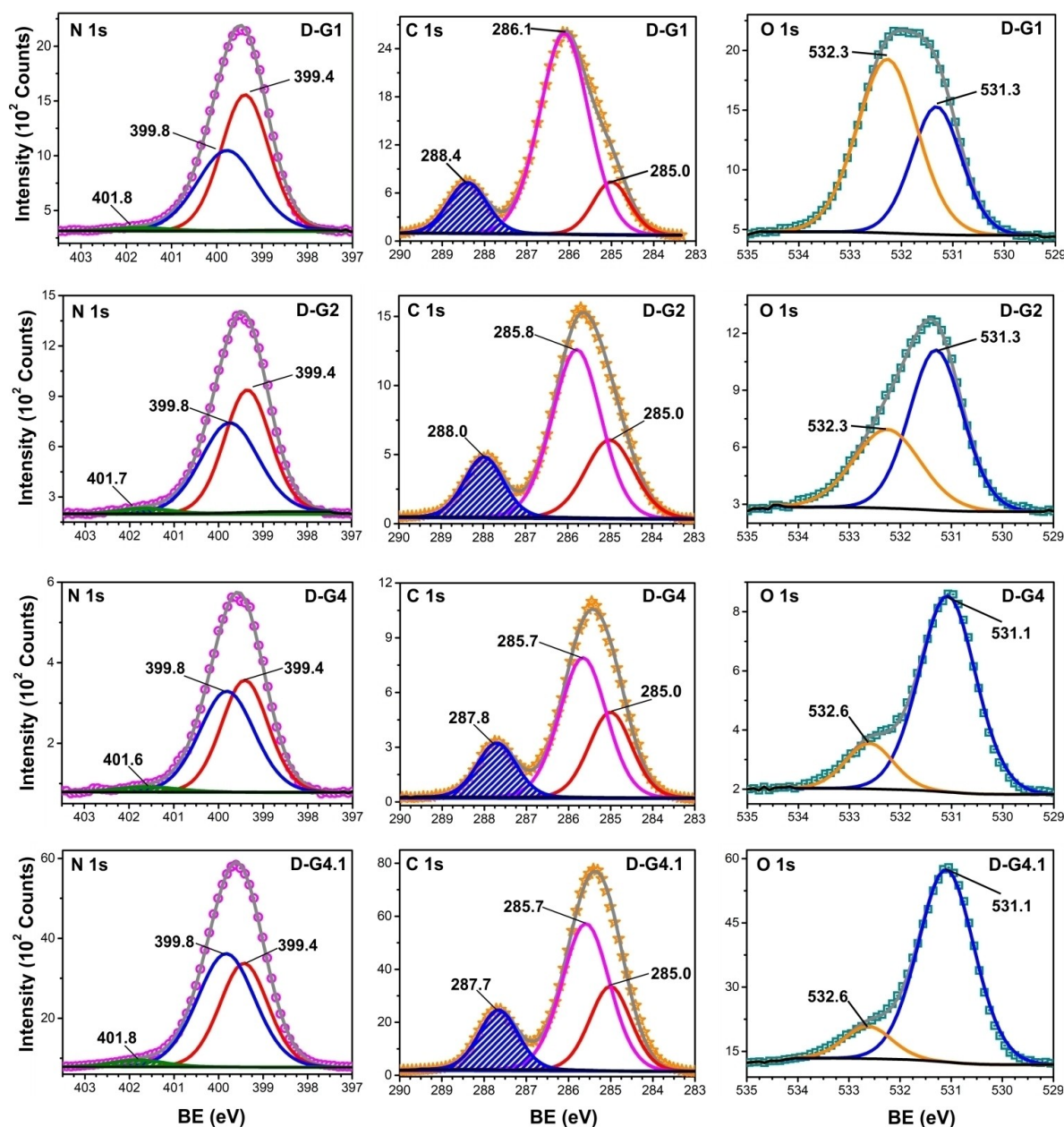
ChemistrySelect

Full Papers
doi.org/10.1002/slct.202000432

**Chemistry
Europe**
European Chemical
Societies Publishing

Figure 5. High-resolution spectra of N1s, C1s and O1s for **D-G1**, **D-G2**, **D-G4** and **D-G4.1** dendrons.

the proportion of dendron functional groups. Besides, the proper amine/amide area ratio indicates the absence of either unreactive free diamine molecules within the samples or cyclization reactions. In this sense, the small variation encountered in **D-G4.1** sample is consistent with the incorporation of Cys molecules through both –NH$_2$ ends, as was suggested previously by TG results. Therefore, this analysis based on XPS can also be suitable for sensing the occurrence and extent of potential defects in the dendron structure.

The high-resolution C 1s signals are depicted in Figure 5 (*center*). The C 1s spectra can be fitted with three main peaks at 285.0, 285.7-286.1 and 287.7-288.4 eV. The first contribution entails the alkyl C–C/CH groups; the second contribution is

assigned to both C–O and C–N bonds, while the third corresponds to the amide carbon in –NH-C=O groups.[8c,34] It is apparent a steadily increase from 10.5 to 18.1% of the amide signal from **D-G1** to **D-G4.1**, which agrees with the successive incorporation of EDA molecules as the dendrons are grown. This contribution also tends to shift to lower binding energies as the dendron generation is increased; such negative shift (around 0.7 eV) is consistent with the occurrence of intra or intermolecular hydrogen bond interactions involving the amide hydrogen, as was previously suggested from the N 1s analysis. Note in all cases the absence of a signal near 289.0 eV typical for the carbonyl carbon of ester groups, which instead is present for the intermediate generations (see Table 5 in the
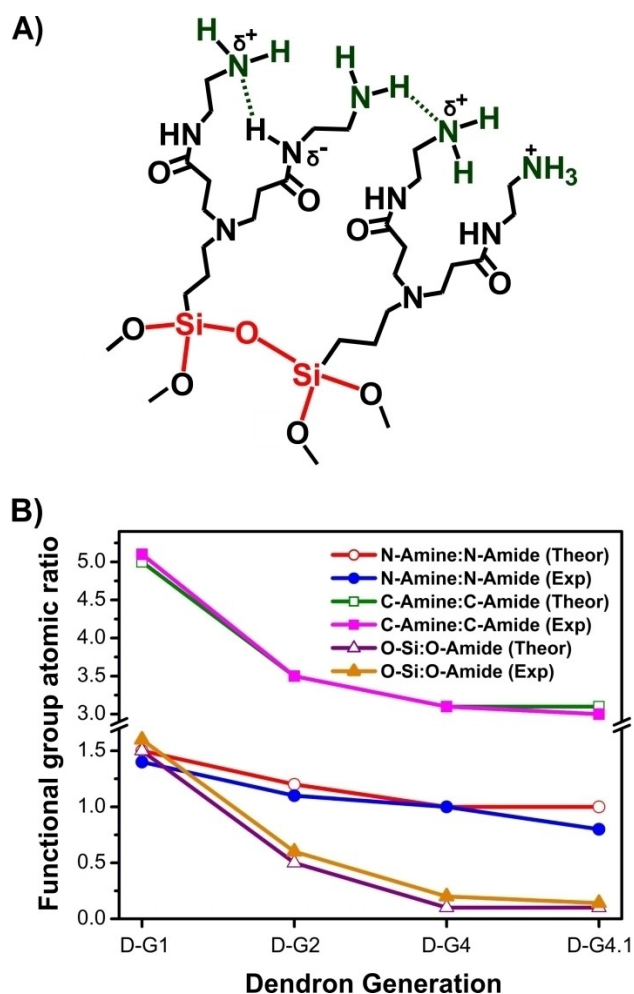
ChemistrySelect

Full Papers
doi.org/10.1002/slct.202000432

Chemistry Europe
European Chemical
Societies Publishing

A)

B)

Figure 6. **A)** Schematic representation of amine interactions within the dendron structure. **B)** Atomic ratio of dendron functional groups as function of dendron generation (*Theor*: theoretical; *Exp*: experimental).

Supporting Information). Hence, dendron defects as unreactive terminal ester groups can also be detected by mean of XPS analysis.

Figure 6B (squares) shows the experimental variation of the area ratio between the second (mostly amine functions) and the third (amide groups) contributions compared with the theoretical values based on the proposed structures. Note that, similar to the results from the N 1s quantification, for all dendron generations there is a close agreement between the experimental XPS data and the expected molecular compositions, which also makes de C 1s high resolution spectrum a solid candidate for monitoring the growth of PAMAM dendrons. A similar result has been reported for the case of G1 PAMAM dendrons anchored on the surface of SiO_2.[20b] Here, it is interesting to underline that the main deviation between both data sets occurs at **D-G4.1** due to an apparent increase in the amide content, which again coincides with the notion of Cys molecules being amidated by the two amine ends.

The high-resolution O 1s signals are depicted in Figure 5 (*right*). Each spectrum can be fitted with two contributions

centred at 531.1-531.3 and 532.3-532.6 eV. The first one accounts for the carboxyl oxygen in the amide group, while the second corresponds to the oxygen atoms in the silane/siloxane core. Since dendron growth does not entail the focal point, it is expected that as the generation gets higher, the amide contribution increases respect to the core contribution, as it is apparent from the spectral sequence and is confirmed in Figure 6 (triangles). In this figure, the theoretical trend expected from the proposed structures is supported by the O1s data. Also, there is no contribution above 533.0 eV, which is indicative of the alkyl O atom of the —O—C≡O groups; this fact suggests the absence of ester functions in the set of complete dendron generations and is in agreement with the C 1s spectra.

Finally, we analysed the S 2p core-level spectrum of the **D-G4.1** sample (see Figure 7). It can be fitted by one contribution with two components separated by 1.2 eV due to the spin orbit coupling. The S $2p_{3/2}$ peak is located at 164.3 eV, which lies in the range for organic disulfides.[34] No sign of sulfide oxidation is observed;[8c] thus the method for the incorporation of disulfide bridges has been proved to be satisfactory since the sulfur function is retained for a future reduction step in order to achieve a PAMAM dendron with terminal thiol and amine groups.

3. Conclusion

In summary, we have developed an efficient methodology for the synthesis of PAMAM-based dendrons with trimethoxysilane as focal point and amine/disulfide functions as terminal groups. The strategy comprises the use of APTMS as reaction core, followed by sequential Michael addition reactions with methyl acrylate and amidation reactions with ethylendiamine, which is substituted in the last step by cystamine in order to introduce peripheral disulfide bridges. Under AFM, the resulting fourth-generation dendrons are seen forming supramolecular structures with ring-like shape; also, they exhibit good colloidal
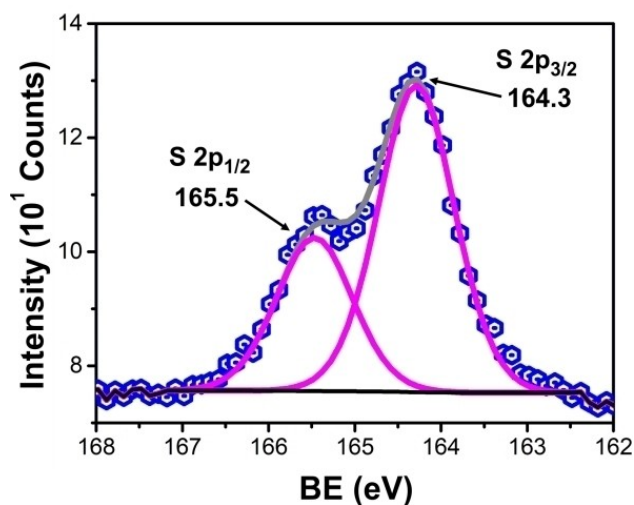

Figure 7. High-resolution spectra of S 2p for **D-G4.1**.

ChemistrySelect

Full Papers
doi.org/10.1002/slct.202000432

**Chemistry
Europe**
European Chemical
Societies Publishing

stability in water bellow pH 6 due to the surface protonation of terminal amine groups. Vibrational spectroscopies confirm the introduction of the desired external functional groups. Detailed XPS analyses reveal that spectral features in the N1s, C1s, O1s and Si 2p signals can be used to monitor the growth of the dendron generations, as well as to detect the occurrence of several defects within the dendron structure during the synthetic steps. Specifically, the sequential increase in the amide content is easily observed through the O 1s C 1s, and N 1s signals; the amine:amide stoichiometry value for the **D-G1**, **D-G2** and **D-G4** samples match very well with those expected for ideal structures. Besides the N 1s signal also allows for the recognition of hydrogen bond interactions comprising the polar groups of the branches and the occurrence of cystamine molecules acting as crosslinking agents within the dendronized structure. The Si 2p signal analysis evidenced the retention of the alkoxysilane core, which tends to hydrolyse and condensate to give dendronized structures linked by siloxanes. Also, we found that the disulfide bridges were successfully introduced for future deprotection of thiol groups. The results from this investigation will be useful for the development and controlling of new versatile PAMAM-based dendrons in order to functionalize advanced materials with hydroxylated surfaces, which will expand their applications in biomedicine, water remediation and industry.

Supporting Information Summary

The Supporting Information contains the Experimental section, including the synthesis of the dendrons and details of the characterization techniques. Also, it includes additional characterization data from TGA, FTIR, STEM, UV-vis and XPS of relevant dendron samples.

Acknowledgements

Conflict of Interest

The authors declare no conflict of interest.

Keywords: Dendrimers · PAMAM · disulfide bridges · alkoxysilanes · Photoelectron Spectroscopy

[1] a) K. Gotoh, E. Shohbuke, Y. Kobayashi, H. Yamada, *Colloids Surf. A* **2018**, *556*, 1–10; b) Y. Han, Y. Liu, W. Wang, J. Leng, P. Jin, *Soft Matter* **2016**, *12*, 2708–2714.

[2] K. L. Mittal, *Polymer surface modification: relevance to adhesion,* Vol. 3, CRC Press, Taylor & Francis Group, Boca Raton, Florida, **2004**.

[3] a) N. V. Katre, *Adv. Drug Delivery Rev.* **1993**, *10*, 91–114; b) T. Keeling-Tucker, M. Rakic, C. Spong, J. D. Brennan, *Chem. Mater.* **2000**, *12*, 3695–3704.

[4] L. Urbano, L. Clifton, H. K. Ku, H. Kendall-Troughton, K.-K. A. Vandera, B. F. Matarese, T. Abelha, P. Li, T. Desai, C. c A Dreiss, *Langmuir* **2018**, *34*, 6125–6137.

[5] a) M. Arkas, D. Tsiourvas, C. M. Paleos, *Macromol. Mater. Eng.* **2010**, *295*, 883–898; b) A. Sengupta, A. K. S. Deb, N. K. Gupta, P. Kumar, K. Dasgupta, S. M. Ali, *J. Radioanal. Nucl. Chem.* **2018**, *315*, 331–340; c) S. Singh, H. Mahalingam, P. K. Singh, *Appl. Catal. A* **2013**, *462*, 178–195; d) H. Viltres, O. F. Odio, E. Reguera, in *Nanohybrids in Environmental & Biomedical Applications* (Ed.: S. K. Sharma), CRC Press, Taylor & Francis Group, Boca Raton, Florida, **2019**, p. 279.

[6] a) S. Staehlke, J. Lehnfeld, A. Schneider, J. B. Nebe, R. Müller, *Mater. Sci. Eng. C* **2019**, *101*, 190–203; b) C. S. R. Vusa, V. Manju, S. Berchmans, P. Arumugam, *RSC Adv.* **2016**, *6*, 33409–33418.

[7] A. Desmecht, T. Steenhaut, F. Pennetreau, S. Hermans, O. Riant, *Chem. Eur. J.* **2018**, *24*, 12992–13001.

[8] a) X. Guo, Y. Feng, X. Lin, Y. Liu, H. Gong, Y. Zhang, *J. Eur. Ceram. Soc.* **2018**, *38*, 1327–1333; b) S. He, H. Wang, C. Zhang, S. Zhang, Y. Yu, Y. Lee, T. Li, *Chem. Sci.* **2019**, *10*, 1816–1822; c) G. Beamson, D. Briggs, *High Resolution XPS of Organic Polymers: The Scienta ESCA300 Database*, Wiley, Chichester, **1992**; d) J. Zhao, M. R. H. S. Gilani, Z. Liu, R. Luque, G. Xu, *Polym. Chem.* **2018**, *9*, 4324–4331.

[9] C. Ornelas, *Macromol. Chem. Phys.* **2016**, *217*, 149–174.

[10] E. Vunain, A. Mishra, B. Mamba, *Int. J. Biol. Macromol.* **2016**, *86*, 570–586.

[11] F. Zeng, S. C. Zimmerman, *Chem. Rev.* **1997**, *97*, 1681–1712.

[12] W. Sun, S. Mignani, M. Shen, X. Shi, *Drug Discovery Today* **2016**, *21*, 1873–1885.

[13] K. Madaan, S. Kumar, N. Poonia, V. Lather, D. Pandita, *J. Pharm. BioAllied Sci.* **2014**, *6*, 139.

[14] K. Liang, H. Yuan, J. Li, J. Yang, X. Zhou, L. He, L. Cheng, Y. Gao, X. Xu, X. Zhou, *Macromol. Mater. Eng.* **2015**, *300*, 107–117.

[15] K. Liu, Z. Xu, M. Yin, *Prog. Polym. Sci.* **2015**, *46*, 25–54.

[16] S. Mousavi, F. Shahraki, M. Aliabadi, A. Haji, F. Deuber, C. Adlhart, *Appl. Surf. Sci.* **2019**, *479*, 608–618.

[17] J. B. Wolinsky, M. W. Grinstaff, *Adv. Drug Delivery Rev.* **2008**, *60*, 1037–1055.

[18] a) S. Wen, K. Li, H. Cai, Q. Chen, M. Shen, Y. Huang, C. Peng, W. Hou, M. Zhu, G. Zhang, *Biomaterials* **2013**, *34*, 1570–1580; b) O. Gansow, C. Wu, M. Brechbiel, in *208th ACS national meeting*, **1994**.

[19] a) Y. Zhu, Y. Niu, H. Li, B. Ren, H. Qu, H. Chen, Y. Zhang, *Ecotoxicol. Environ. Saf.* **2018**, *162*, 253–260; b) Y. X. Ma, W. J. Shao, P. S. Jin, Y. L. Kou, X. Li, *Polym. Compos.* **2019**, *40*, E1685-E1696.

[20] a) C. Demathieu, M. M. Chehimi, J.-F. Lipskier, A.-M. Caminade, J.-P. Majoral, *Appl. Spectrosc.* **1999**, *53*, 1277–1281; b) M. Sharma, A. Dube, J. R. Engstrom, *J. Am. Chem. Soc.* **2007**, *129*, 15022–15033.

[21] L. Tao, G. Chen, G. Mantovani, S. York, D. M. Haddleton, *Chem. Commun.* **2006**, 4949–4951.

[22] H. F. Gilbert, *Methods Enzymol.* **1995**, *251*, 8–28.

[23] G. Ferrer-Sueta, B. Manta, H. Botti, R. Radi, M. Trujillo, A. Denicola, *Chem. Res. Toxicol.* **2011**, *24*, 434–450.

[24] a) J. Yang, H.-D. Wang, S.-X. Xu, G.-X. Li, Y.-J. Huang, *J. Polym. Res.* **2005**, *12*, 317–323; b) O. F. Odio, L. Lartundo-Rojas, E. G. Palacios, R. Martínez, E. Reguera, *Appl. Surf. Sci.* **2016**, *386*, 160–177.

[25] K. Xu, W. Sun, Y. Shao, F. Wei, X. Zhang, W. Wang, P. Li, in *Nanotechnol. Rev.* **2018**, *7*, 605.

[26] a) A. Deffieux, M. Schappacher, A. Hirao, T. Watanabe, *J. Am. Chem. Soc.* **2008**, *130*, 5670–5672; b) J. Li, L. T. Piehler, D. Qin, J. R. Baker, D. A. Tomalia, D. J. Meier, *Langmuir* **2000**, *16*, 5613–5616.

[27] a) C. Kaewtong, G. Jiang, M. J. Felipe, B. Pulpoka, R. Advincula, *ACS Nano* **2008**, *2*, 1533–1542; b) D. Xie, M. Jiang, G. Zhang, D. Chen, *Chem. Eur. J.* **2007**, *13*, 3346–3353.

[28] a) T. Müller, D. G. Yablon, R. Karchner, D. Knapp, M. H. Kleinman, H. Fang, C. J. Durning, D. A. Tomalia, N. J. Turro, G. W. Flynn, *Langmuir* **2002**, *18*, 7452–7455; b) T. A. Betley, M. M. Banaszak Holl, B. G. Orr, D. R. Swanson, D. A. Tomalia, J. R. Baker, *Langmuir* **2001**, *17*, 2768–2773.

[29] D. A. Tomalia, A. M. Naylor, W. A. Goddard III, *Angew. Chem. Int. Ed. Engl.* **1990**, *29*, 138–175.

[30] a) L. A. O'Hare, A. Hynes, M. R. Alexander, *Surf. Interface Anal.: An International Journal devoted to the development and application of*

techniques for the analysis of surfaces, interfaces and thin films **2007**, *39*, 926–936; b) R. A. Shircliff, P. Stradins, H. Moutinho, J. Fennell, M. L. Ghirardi, S. W. Cowley, H. M. Branz, I. T. Martin, *Langmuir* **2013**, *29*, 4057–4067; c) C. A. Szafranski, W. Tanner, P. E. Laibinis, R. L. Garrell, *Langmuir* **1998**, *14*, 3570–3579.

[31] a) B. Qiao, T.-J. Wang, H. Gao, Y. Jin, *Appl. Surf. Sci.* **2015**, *351*, 646–654; b) L. White, C. Tripp, *J. Colloid Interface Sci.* **2000**, *232*, 400–407.

[32] a) M. H. Ahmed, J. A. Byrne, J. McLaughlin, A. Elhissi, W. Ahmed, *Appl. Surf. Sci.* **2013**, *273*, 507–514; b) J. Liu, T. Zhang, Z. Wang, G. Dawson, W. Chen, *J. Mater. Chem.* **2011**, *21*, 14398–14401; c) P. G. Rouxhet, M. J. Genet, *Surf. Interface Anal.* **2011**, *43*, 1453–1470; d) G. Tzvetkov, F. P. Netzer, *J. Chem. Phys.* **2011**, *134*, 204704.

[33] a) R. G. Acres, A. V. Ellis, J. Alvino, C. E. Lenahan, D. A. Khodakov, G. F. Metha, G. G. Andersson, *J. Phys. Chem. C* **2012**, *116*, 6289–6297; b) H. Min, P.-L. Girard-Lauriault, T. Gross, A. Lippitz, P. Dietrich, W. E. Unger, *Anal. Bioanal. Chem.* **2012**, *403*, 613–623; c) E. T. Vandenberg, L. Bertilsson, B. Liedberg, K. Uvdal, R. Erlandsson, H. Elwing, I. Lundström, *J. Colloid Interface Sci.* **1991**, *147*, 103–118; d) F. Zhang, M. Srinivasan, *Langmuir* **2004**, *20*, 2309–2314.

[34] a) A. V. Naumkin, A. Kraut-Vass, S. W. Gaarenstroom, C. J. Powell, "NIST X-ray Photoelectron Spectroscopy Database, NIST Standard Reference Database 20, Version 4.1", can be found under https://srdata.nist.gov/xps/Default.aspx, **2012**.